PERGAMON

International Journal of Multiphase Flow 27 (2001) 1029–1049

International Journal of Multiphase Flow

www.elsevier.com/locate/ijmulflow

Onsets of entrainment during dual discharge from a stratified two-phase region through horizontal branches with centrelines falling in an inclined plane: Part 2 – Experiments on gas and liquid entrainment

M.R. Maier, H.M. Soliman *, G.E. Sims

Department of Mechanical and Industrial Engineering, University of Manitoba, Winnipeg, Man., Canada R3T 5V6

Received 3 August 1999; received in revised form 1 October 2000

Abstract

An experimental investigation has been conducted for determining the critical height and the location for the onset of gas and liquid entrainment during dual discharge from a stratified air–water region through branches mounted on a vertical wall. The two branches are horizontal, have circular cross-section (6.35 mm i.d.), and their centrelines fall in a common plane with variable inclinations from the horizontal. Effects of the separating distance between the branches, the flow rates through the branches, and the inclination angle of the plane containing the centrelines of the branches on the critical height and the location of the onset of both phenomena are presented and discussed. Comparisons between the present data of liquid entrainment and the finite-branch analysis presented in Part 1of this paper show good agreement.

Keywords: Experimental data; Dual discharge; Gas and liquid entrainment; Branches falling in an inclined plane

1. Introduction

The importance of two-phase discharge from stratified regions, due to its relevance to many industrial applications (as pointed out in Part 1 of this paper), has motivated several experimental investigations for determining the onsets of gas and liquid entrainment using different discharge configurations. Knowledge of the critical height of the gas–liquid interface at both onsets under different operating conditions is required because the type of discharging flow (single or two-

* Corresponding author. Tel.: +1-204-474-9307; fax: +1-204-275-7507.
E-mail address: hsolima@cc.umanitoba.ca (H.M. Soliman).

0301-9322/01/$ - see front matter
PII: S0301-9322(00)00060-4

phase) can then be related to the height of the interface. This is a prerequisite for being able to determine the mass flow rate and quality of the discharging flow.

Detailed experiments were reported on the onsets of gas and liquid entrainment, two-phase mass flow rate and quality during single discharge from a large stratified region (e.g., Smoglie and Reimann, 1986; Schrock et al., 1986; Yonomoto and Tasaka, 1988, 1991; Micaelli and Memponteil, 1989; Hassan et al., 1998).

A number of studies were reported in the literature dealing with the situation of multiple discharge from a stratified two-phase region. Parrott et al. (1991) reported experimental data for the onset of gas entrainment during dual discharge from horizontal branches mounted on a vertical wall with the centrelines of the branches falling in a common vertical plane. For this geometry, Armstrong et al. (1992) developed a theoretical model and experimental data for the onset of liquid entrainment with excellent agreement between data and theory. Later, Hassan et al. (1996a) extended the work on this geometry to include measurements of the mass flow rate and quality in the two branches. Further experimental data were reported for the onsets of gas and liquid entrainment, mass flow rate and quality during discharge from two horizontal branches with centrelines falling in a common horizontal plane (Hassan et al., 1996b), as well as discharge from three branches mounted on a semicircular wall (Hassan et al., 1997).

In distribution headers and multi-passage heat exchangers, the outlet branches can be located at various positions relative to each other. The objective of this investigation is to develop experimental data for the onsets of gas and liquid entrainment during discharge from a stratified region through two horizontal branches mounted on a vertical wall with the centreline of the branches falling in a common inclined plane. The present data for the onset of liquid entrainment will be compared with the theoretical predictions developed in Part 1 of this paper.

2. Experimental investigation

2.1. Experimental parameters

Fig. 1 shows the geometrical and flow parameters relevant to the experiments on gas and liquid entrainment. Two branches of equal diameter d and a separating distance L (centre-to-centre) are placed on the side of a large reservoir containing stratified layers of air and water at a pressure P_0. In both type of experiments (gas and liquid entrainment), the primary branch (branch 1) is closer to the gas–liquid interface than the secondary branch (branch 2). The plane containing the centrelines of the two branches is inclined an angle α from the horizontal. The single-phase mass flow rates through branches 1 and 2 are $\dot{m}_1$ and $\dot{m}_2$, respectively. This single-phase flow is gas (air) in the liquid entrainment experiments and liquid (water) in the gas entrainment experiments.

The onset of gas or liquid entrainment is the point when the single-phase flow in one of the two branches, or both simultaneously, just becomes two-phase. At the onset, the vertical distance between the flat interface (away from the wall) and a horizontal plane passing through the centreline of branch 1 is the critical height h. Location of the onset (branch 1, branch 2, or both

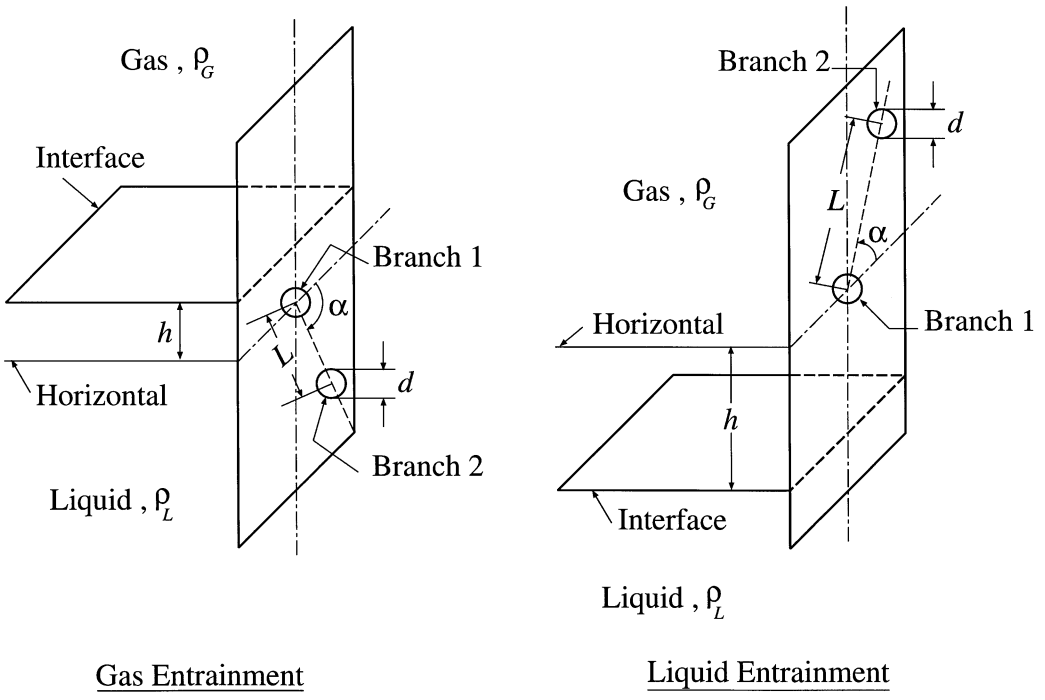

Fig. 1. Relevant geometrical and flow parameters.

branches simultaneously) and the magnitude of h would be dependent on $\dot{m}_1, \dot{m}_2, L, d, \rho_L, \rho_G$, and α, where ρ_L and ρ_G are the liquid and gas densities, respectively. This list of independent variables is based on the assumption that viscosity and surface tension have negligible effects on both phenomena.

Performing a simple dimensional analysis of the problem, it is possible to identify h/d, Fr_1, Fr_2, L/d, and α, as the relevant dimensionless groups, where Fr_1 and Fr_2 are the Froude numbers for branches 1 and 2, respectively, given by

$$Fr_i = \frac{(4/\pi)\dot{m}_i}{\sqrt{gd^5\rho_C(\rho_L - \rho_G)}}, \quad i = 1, 2. \tag{1}$$

In Eq. (1), g is the gravitational acceleration and ρ_C is the density of the continuous phase through the branch ($\rho_C = \rho_L$ in gas entrainment experiments and $\rho_C = \rho_G$ in liquid entrainment experiments). The correlations for the onsets of gas and liquid entrainment would, therefore, take the form

$$h/d = f(Fr_1, Fr_2, L/d, \alpha). \tag{2}$$

The objective of the present experimental investigation is to study the dependence of h/d on each of the four independent variables listed in Eq. (2). The experimental data on liquid entrainment will be compared with the theoretical predictions obtained in Part 1 of this paper (Maier et al., 2001).

2.2. Experimental apparatus

Fig. 2 shows a schematic diagram of the flow loop used in the gas entrainment experiments. An immersion-type circulating pump was used to supply distilled water to the test section at a rate controlled by a by-pass line. The temperature of the water was held steady (near room temperature) by a cooling coil immersed in the water tank. The test section was connected to an air supply equipped with a feed-back pressure controller which maintained the test-section pressure, P_0, steady at a preset value.

The test section is basically a large reservoir in the shape of a tee, manufactured from schedule 40 stainless-steel sections. It had a clear acrylic-pipe section near the outlet flange for visual observation of the flow phenomena. The tee measured approximately 1.1 m in length from the air inlet flange to the discharge flange. The inner diameter was approximately 0.255 m in all sections, except the visual section, which measured 0.28 m. The distance from the horizontal centreline of the tee to the water inlet flange was approximately 0.516 m. In order to attain a smooth, ripple-free interface, the water and air inlet flows were dispersed as they entered the test section. A detailed cross-sectional view of the test section can be found in Parrott et al. (1991).

The discharge branches were holes, 6.35 mm dia. and 127 mm long, machined in brass blocks. Thus, each branch had a straight length of 20 dia. before any bends or area changes were incorporated. Two brass blocks were used: one with two branches machined to provide $L/d = 1.5$ and the other with four branches machined for $L/d = 2$ and 8. Fig. 3 shows a layout of the block used for $L/d = 2$ and 8. Depending on the desired L/d, one of the two blocks was bolted to the outlet flange of the test section with the inside brass surface flush to the inside surface of the outlet flange. A surveying transit was used to ensure that the faces of the flange and the block were vertical. Slots were machined in the mounting flange of the brass blocks that allowed rotation of

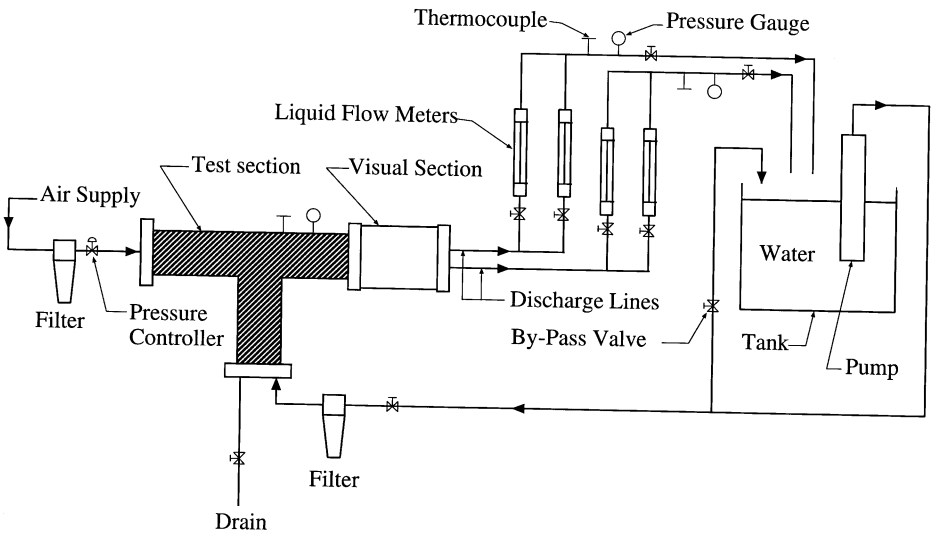

Fig. 2. Schematic diagram of the flow loop for gas-entrainment experiments.

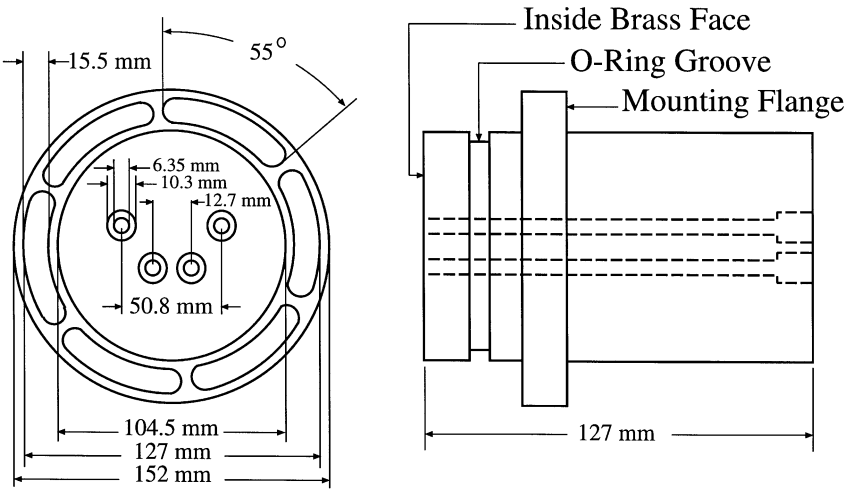

Fig. 3. Branch layout in the brass block for $L/d = 2$ and 8.

the block so that the whole range of angles, $0° \leqslant \alpha \leqslant 90°$, could be covered. A circular protractor was mounted on the outer surface of the brass-block mounting flange for measuring α and the datum ($\alpha = 0°$) was determined by a surveying transit. Two pressure taps, one on the air side and the other on the water side, were installed on the outlet flange and connected to a differential pressure transducer in order to measure the liquid height in the test section.

The outlet water flow rate from each branch was measured by two variable-area-type flow meters with overlapping ranges covering flow rates from 0.51 to 41.34 l/min. The rate of discharge from each branch was controlled by throttling valves located just downstream of the flow meters. The pressure and temperature were measured upstream of the throttling valve and in the test section. All flow meters, thermocouples, and pressure gauges were calibrated before testing began.

The flow loop was slightly modified for the liquid entrainment experiments. The water rotameters were replaced by air rotameters (two for each branch with overlapping ranges) covering flow rates from 16.65 to 1300 standard l/min. An air–water separator was installed on each branch upstream on the air rotameters to prevent any entrained liquid from wetting the rotameters. Also, a mercury manometer was installed on each line between the rotameters and the throttling valve in order to provide an accurate reading of air pressure flowing in the rotameters. The air rotameters were calibrated before testing began.

2.3. Experimental procedure and data reduction

The testing program for both gas and liquid entrainment was designed to provide quantitative assessment of the influences of Fr_2, L/d, and α on the location of the onset and the value of h/d over a wide range of Fr_1. Thus, the test matrix for both onsets included four values of Fr_2, three values of L/d, and four values of α. In each data set corresponding to a combination of Fr_2, L/d, and α, several data points were generated covering the widest possible range of Fr_1. The procedure followed in generating each datum point is given in the following sections.

2.3.1. Gas entrainment experiments

1. The atmospheric pressure and room temperature were recorded.
2. The test section was filled with water far above both branches and the test section was charged with compressed air in order to maintain a steady pressure of 510 kPa.
3. Water flow through the outlet branches was initiated and the desired values of Fr_1 and Fr_2 were set by adjusting the throttling valves downstream of the rotameters.
4. The interface level was lowered slowly by adjusting the valve in the by-pass line downstream from the pump. Typically, the interface dropped by less than 1 mm/min.
5. When, by visual observation through the acrylic-pipe section, a stable gas cone formed that was continuously entraining and not breaking off from the branch(es), the onset of entrainment was said to have occurred. At this moment, the transducer reading was taken (from which h/d was determined) and the branch(es) at which entrainment occurred was recorded.
6. Other readings taken immediately after the onset were the test-section pressure, the air and water temperatures inside the test section, and the water temperature downstream of the rotameters. The value of ρ_L was determined from the water temperature downstream of the rotameters and the value of ρ_G was determined from the pressure and temperature of the air inside the test section assuming ideal gas behaviour. Froude numbers Fr_1 and Fr_2 were calculated from Eq. (1).

A special effort was made for establishing the simultaneous point. For fixed Fr_2, L/d, and α, the value of Fr_1 was iterated in order to determine the simultaneous entrainment point exactly. The inside face of the brass block was cleaned on a regular basis with a 0.3 μm cleaning compound and alcohol to remove oxidation and ensure the surface was smooth.

2.3.2. Liquid entrainment experiments

1. The atmospheric pressure and room temperature were recorded.
2. The test section was filled with water far below both branches and the test section was charged with compressed air maintaining a steady pressure of 310 kPa.

Table 1
Experimental test matrix

Fr_2 for gas entrainment	Fr_2 for liquid entrainment	L/d	$\alpha = 0°$	$\alpha = 10°$	$\alpha = 30°$	$\alpha = 60°$
14.0	9.5	1.5	X	X	X	X
		2.0	X	X	X	X
		8.0	X	X	X	
28.5	19.0	1.5	X	X	X	X
		2.0	X	X	X	X
		8.0	X	X	X	
42.5	28.5	1.5	X	X	X	X
		2.0	X	X	X	X
		8.0	X	X	X	
56.6	38.0	1.5	X	X	X	X
		2.0	X	X	X	X
		8.0	X	X	X	

3. Air flow through the outlet branches was initiated and the desired values of Fr_1 and Fr_2 were set by adjusting the throttling valves downstream of the rotameters. The brass block was allowed to dry thoroughly by the air flow.
4. The interface level was raised slowly by adjusting the valve in the by-pass line downstream from the pump. Typically, the interface was raised by less than 1 mm/min.

Fr_2 for Gas Entrainment	0	14.9					28.5					42.5					56.6				
Fr_2 for Liquid Entrainment	0	9.5					19.0					28.5					38.0				
Symbol	✳	○	⊙	⊕	⊖	●	△	◬	⏃	⏢	▲	□	⊡	⊞	⊟	■	◇	◈	⊕	⊖	◆
Category		1	2	3	4	5	1	2	3	4	5	1	2	3	4	5	1	2	3	4	5

Fig. 4. Legend for Figs. 5–16.

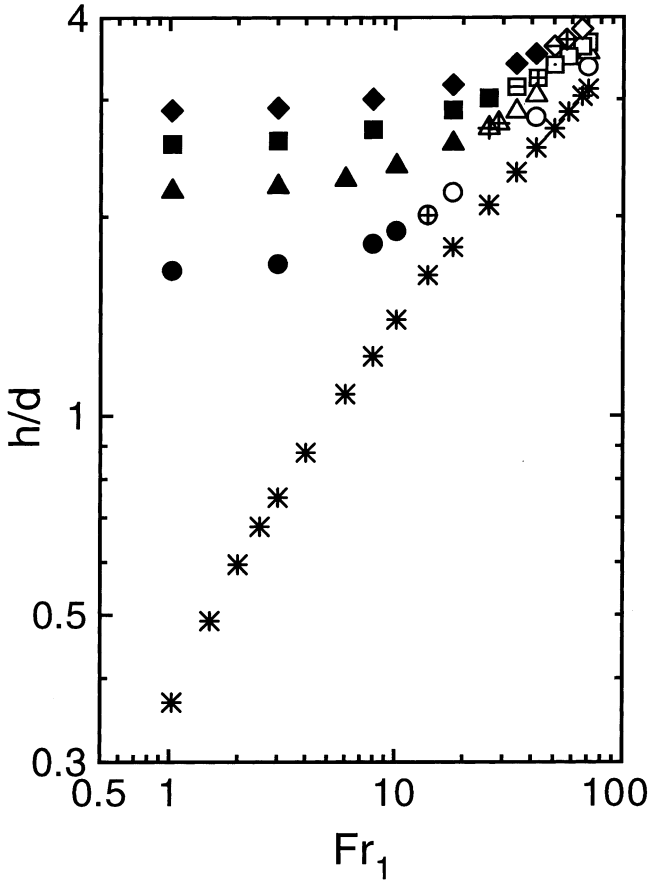

Fig. 5. Gas-entrainment data for $L/d = 1.5$ and $\alpha = 0°$.

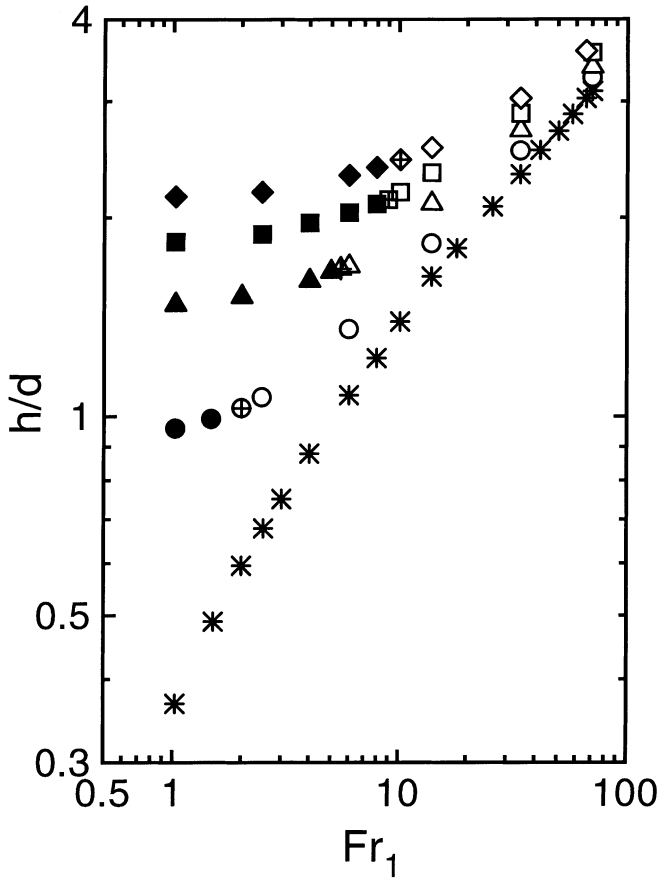

Fig. 6. Gas-entrainment data for $L/d = 1.5$ and $\alpha = 30°$.

5. When, by visual observation, a liquid spout was pulled up the test piece and entrained continuously into the branch(es), the onset of entrainment was said to have occurred. At this moment, the transducer reading was taken (for calculating h/d) and the branch(es) at which entrainment occurred was recorded.
6. Other readings taken immediately after the onset were the air pressure and temperature inside the test section, P_0 and T_0, respectively, the water temperature inside the test section (which gave the value of ρ_L), and the air temperature and pressure downstream from the air rotameters (these readings, together with the rotameters'readings gave $\dot{m}_1$ and $\dot{m}_2$).

For all data points, the floats in the rotameter were very steady, the pressure transducer's signal free from noise, and the brass block thoroughly dried between points. Similar to the case of gas entrainment, iteration of Fr_1 was required to accurately determine the point of simultaneous entrainment for fixed values of Fr_2, L/d, and α. As well, the brass-block surface was cleaned regularly to ensure that its surface condition was controlled throughout the study.

The above procedure produced values for the mass flow rates $\dot{m}_1$ and $\dot{m}_2$, the critical height h, and the stagnation conditions within the test section P_0 and T_0. To calculate the Froude numbers

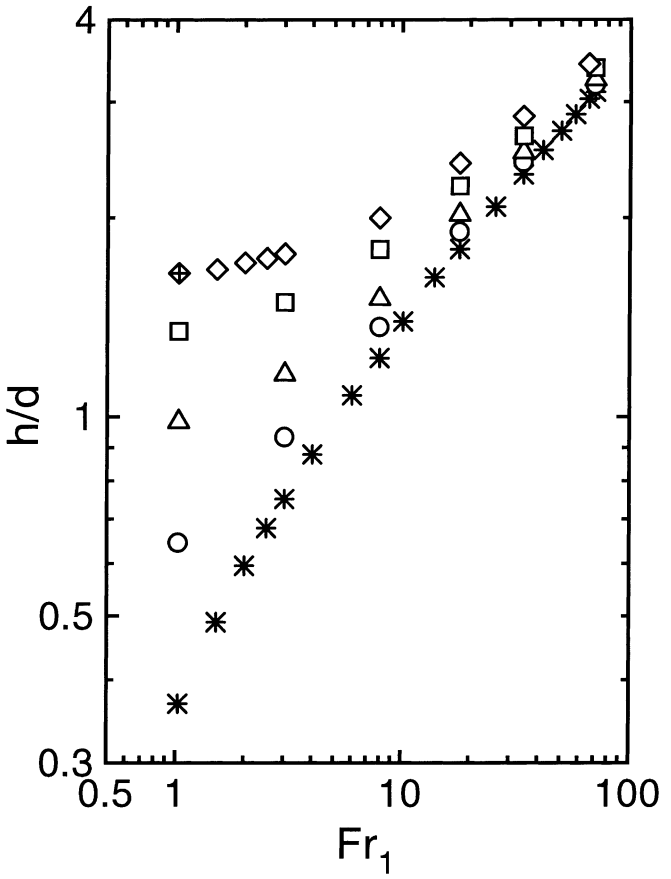

Fig. 7. Gas-entrainment data for $L/d = 1.5$ and $\alpha = 60°$.

at each branch inlet, Fr_1 and Fr_2, the air densities at the inlet of the branches, ρ_{G1} and ρ_{G2}, were required. This was done by applying the following procedure for each branch:

1. An energy balance was applied between the stagnation conditions and the branch inlet assuming ideal gas behaviour, thus giving

$$C_p T_0 = C_p T + 8\left(\frac{\dot{m}}{\pi \rho_G d^2}\right)^2, \tag{3}$$

where C_p is the constant-pressure specific heat and T is the temperature at branch inlet.

2. The density was formulated as

$$\rho_G = \frac{P}{RT}, \tag{4}$$

where P is the pressure at branch inlet and R is the ideal gas constant for air.

3. The expansion from stagnation conditions to branch inlet was assumed to be isentropic, thus

$$T/T_0 = (P/P_0)^{(k-1)/k}, \tag{5}$$

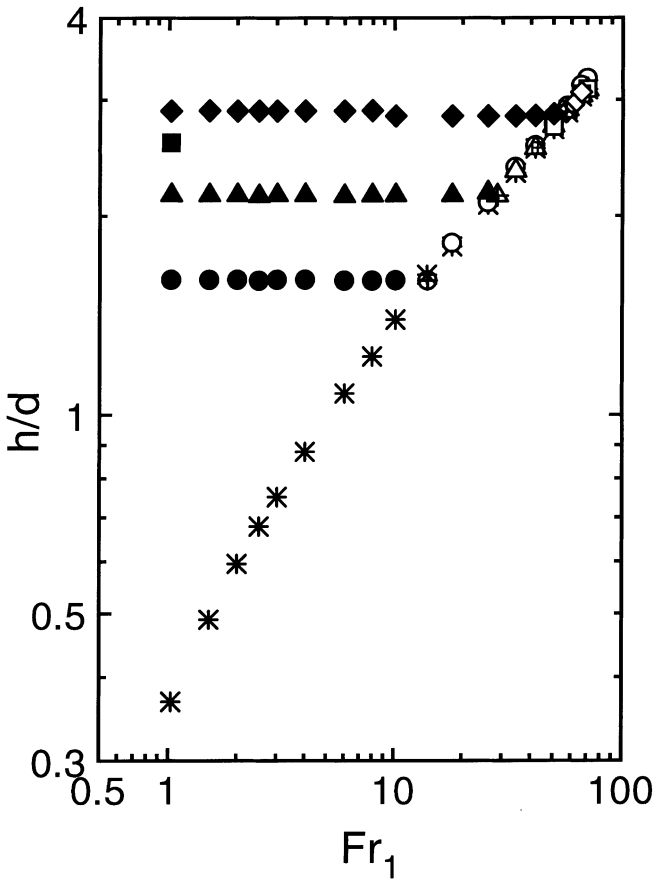

Fig. 8. Gas-entrainment data for $L/d = 8.0$ and $\alpha = 0°$.

where k is the ratio of specific heats for air.

Eqs. (3)–(5) were solved iteratively for the values of P, T, and ρ_G. Definition (1) was then used for the evaluation of Fr for each branch.

2.4. Estimates of experimental uncertainty

An uncertainty analysis was performed for gas and liquid entrainment experiments. The uncertainty analysis was performed following the approach of Kline and McClintock (1953). The uncertainty analysis was performed for six representative data sets; three for gas entrainment and three for liquid entrainment. The reason for performing an abbreviated uncertainty analysis stems from the fact that the experimental apparatus was used in previous studies. The uncertainty in the data obtained from the experimental rig has been established by Parrott (1993) and Hassan (1995).

The uncertainty in Froude number during the gas entrainment experiments for the data sets examined ranged from $\pm 3.3\%$ to $\pm 4.8\%$. The uncertainty in the branch diameter and the uncertainty in the volumetric flow rate through the flowmeters were the dominant uncertainties in the Froude number.

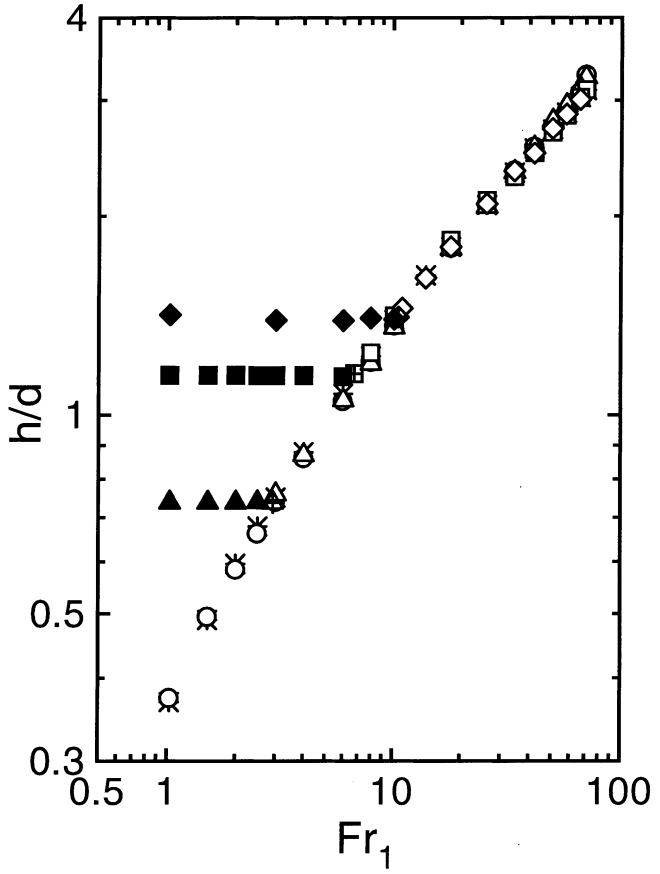

Fig. 9. Gas-entrainment data for $L/d = 8.0$ and $\alpha = 10°$.

The uncertainty in Froude number during the liquid entrainment experiments for the data sets examined ranged from ±4.0% to ±8.7%. The uncertainty in the branch air-inlet density and the uncertainty in the volumetric flow rate through the flowmeters dominated the uncertainty in the Froude number.

The uncertainty in the critical height for gas entrainment ranged from ±1.9% to ±5.4%. The uncertainty in the critical height for liquid entrainment ranged from ±1.9% to ±3.1%.

3. Results and discussion

3.1. Flow phenomena

Early in the experimental program, a complete description of all observed flow phenomena at or near the onset of entrainment was recorded for all data points (Maier, 1998). After careful examination of these observations, it was decided to classify the data points into five categories that ensured high degree of repeatability in the data. These categories apply to both gas and liquid entrainment, and they can be described as follows:

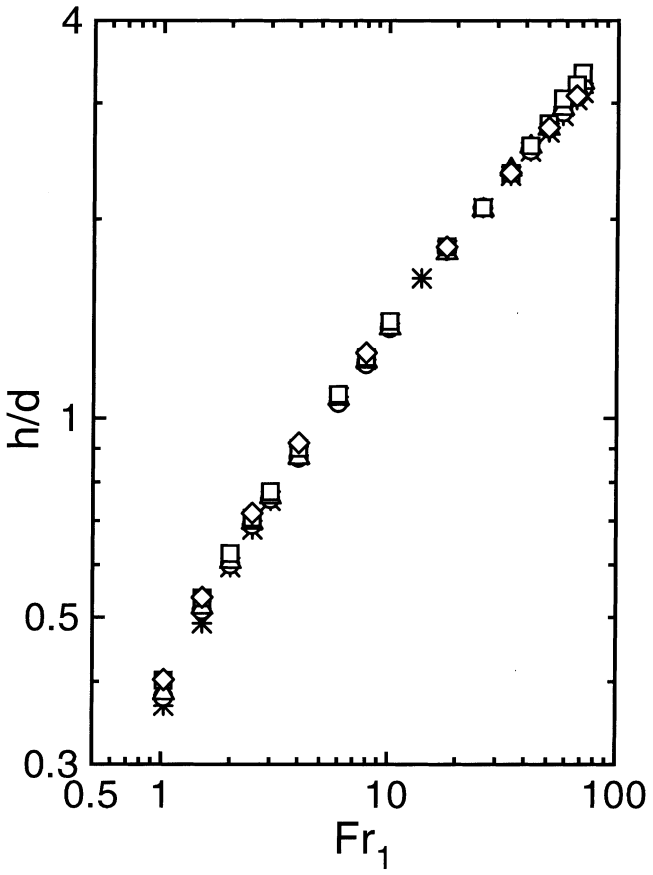

Fig. 10. Gas-entrainment data for $L/d = 8.0$ and $\alpha = 30°$.

Category 1 (Entrainment at branch 1). The onset of continuous entrainment occurred at branch 1 only.

Category 2 (Entrainment at branch 1 with intermittence at branch 2). The onset of continuous entrainment occurred at branch 1 with intermittent entrainment at branch 2.

Category 3 (Simultaneous entrainment). The onset of continuous entrainment occurred at the same instance at branches 1 and 2.

Category 4 (Entrainment at branch 2 with intermittence at branch 1). The onset of continuous entrainment occurred at branch 2 with intermittent entrainment at branch 1.

Category 5 (Entrainment at branch 2). The onset of continuous entrainment occurred at branch 2 only.

In the gas entrainment experiments, both vortex and vortex-free gas cones were observed.

3.2. Test conditions

An extensive matrix of data was collected to ensure that the onset phenomena were well investigated under wide ranges of test conditions. All tests were conducted at room temperature and

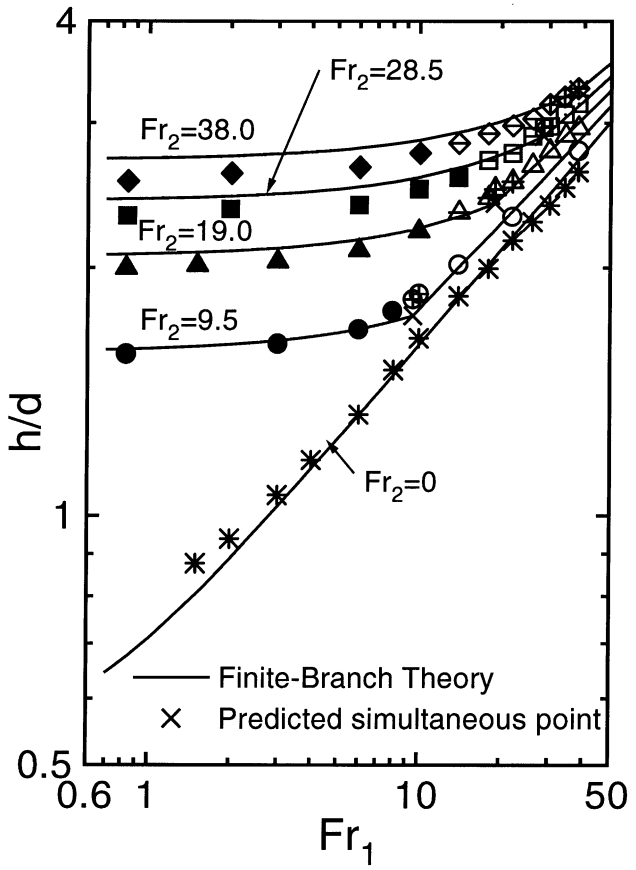

Fig. 11. Experimental data and theoretical predictions of liquid-entrainment for $L/d = 1.5$ and $\alpha = 0°$.

all branches had a size $d = 6.35$ m. The gas entrainment tests were conducted at $P_0 = 510$ kPa, while the liquid entrainment tests were done at $P_0 = 310$ kPa.

The test matrix is shown in Table 1. For each type of entrainment, four values of Fr_2, three values of L/d, and four values of α were used. The total number of combinations of Fr_2, L/d, and α used in each type of entrainment was 44. For each combination, several data points were generated in order to cover the widest possible range of Fr_1. In addition, data for the case of a single branch were also generated for gas and liquid entrainment ($Fr_2 = 0$).

3.3. Gas entrainment

Fig. 5 shows the data for the onset of gas entrainment corresponding to $L/d = 1.5$ and $\alpha = 0°$. A common legend is given in Fig. 4 for interpreting the results in Figs. 5–16 based on the entrainment categories described in Section 3.1. Considering the data for $Fr_2 = 42.5$ in Fig. 5, we notice that entrainment Category 5 is encountered for $1 \leqslant Fr_1 \leqslant 26$ with slightly increasing h/d with Fr_1. At $Fr_1 = 34$, the onset phenomenon changes to Category 4, while simultaneous entrainment (Category 3) is encountered at $Fr_1 = Fr_2 = 42.5$ (since $\alpha = 0°$). At $Fr_2 = 50.1$, the

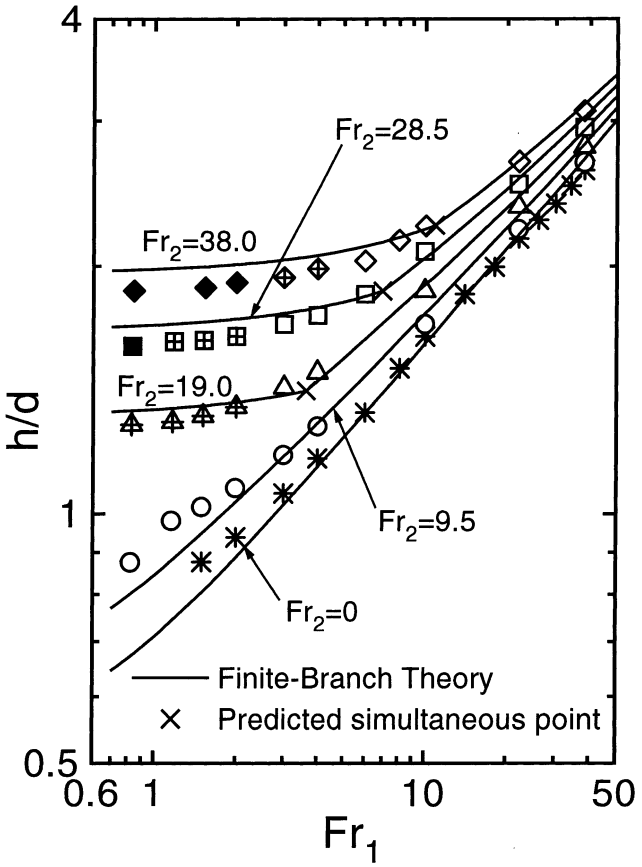

Fig. 12. Experimental data and theoretical predictions of liquid-entrainment for $L/d = 1.5$ and $\alpha = 30°$.

entrainment mode shifts to Category 2, while Category 1 entrainment was observed for $57.7 \leqslant Fr_1 \leqslant 70.3$. In general, Categories 2–4 occupy bands of finite widths on the Fr_1 scale. As well, Fig. 5 shows that h/d increases as Fr_1 and/or Fr_2 increase for fixed L/d and α.

Figs. 6 and 7, together with Fig. 5, illustrate the effect of α on h/d for fixed L/d of 1.5. It can be noted that all entrainment categories shift to lower Fr_1 as α increases. As a matter of fact, most of the data in Fig. 7 ($\alpha = 60°$) correspond to Category 1, while most of the data in Fig. 5 ($\alpha = 0°$) are of Category 5. We also note that h/d decreases as α increases for the same Fr_1, Fr_2, and L/d.

The results presented so far correspond to a small branch separation ($L/d = 1.5$) and the trends for $L/d = 2$ are similar to those seen in Figs. 5–7 (Maier, 1998). These results indicate mutual interaction between the branches due to their proximity to each other. For large branch separation ($L/d = 8$), the results for $\alpha = 0°$, 10° and 30° are presented in Figs. 8–10, respectively. These results show that entrainment Categories 2 and 4 disappear at this large value of L/d. For any finite value of Fr_2 in Fig. 8, entrainment Category 5 occurs at the lower values of Fr_1 with practically a constant value of h/d. As Fr_1 increases, entrainment shifts to Category 3 at the single-discharge line. From that point, as Fr_1 increases further, entrainment shifts to Category 1 with values of h/d following closely the single-discharge line. This behaviour suggests that the two

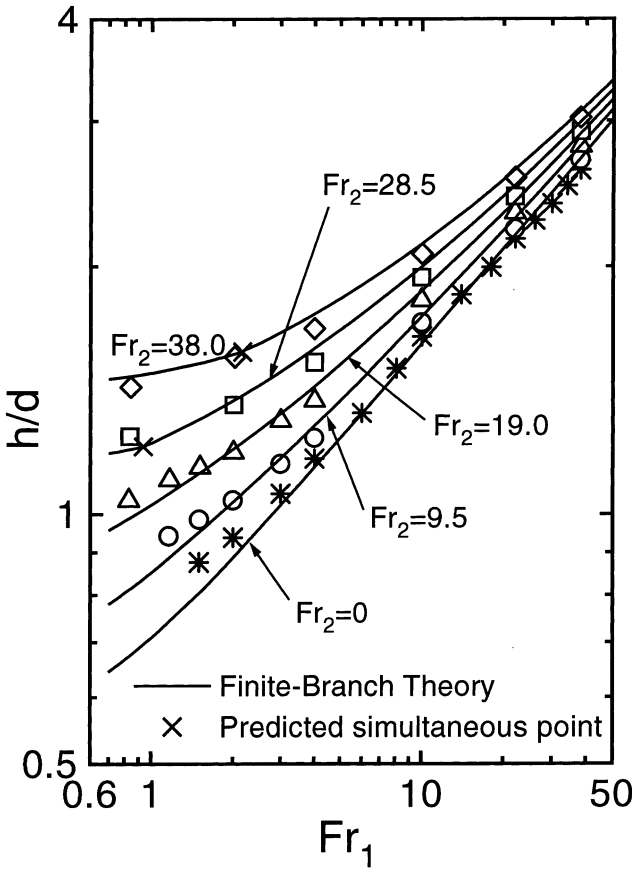

Fig. 13. Experimental data and theoretical predictions of liquid-entrainment for $L/d = 1.5$ and $\alpha = 60°$.

branches are acting independently with very small (if any) effect of the flow from one branch on the other. The trend of decreasing h/d with α is also evident in Figs. 8–10. As well, the shift of the simultaneous point to lower Fr_1 as α increases is clear from these figures. For $\alpha = 30°$ and $L/d = 8$ (Fig. 10), all the data for $1 \leqslant Fr_1 \leqslant 70$ correspond to entrainment Category 1; i.e., entrainment at branch 1, with values of h/d very close to the single-discharge values. This is a further confirmation of the trend that the two branches become independent of each other.

3.4. Liquid entrainment

The experimental results for the onset of liquid entrainment are shown in Figs. 11–13 for $L/d = 1.5$ and in Figs. 14–16 for $L/d = 8$. The results for $L/d = 2$ are similar in trend to those for $L/d = 1.5$ and, therefore, not presented here. The theoretical values of h/d, including the location of the simultaneous point, as predicted by the finite-branch analysis in Part 1 of this paper are shown in all figures.

Figs. 11–13 for $L/d = 1.5$ show that h/d increases as Fr_1 and/or Fr_2 increase, whether the entrainment is at branch 1 (Category 1) or at branch 2 (Category 5). This trend confirms the mutual

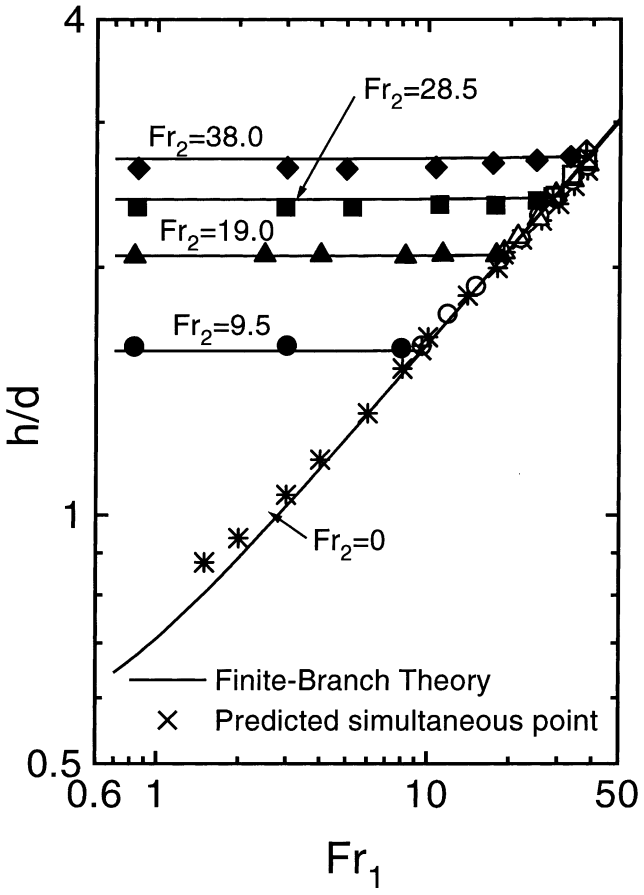

Fig. 14. Experimental data and theoretical predictions of liquid-entrainment for $L/d = 8.0$ and $\alpha = 0°$.

interaction between the branches. As α increases, all entrainment categories shift to lower Fr_1, similar to the gas entrainment case. As well, h/d decreases as α increases, particularly for Category 5 entrainment. For $\alpha = 0°$, Fig. 11 shows that all five categories of entrainment were observed, while for $\alpha = 30°$, Categories 2 and 4 were not observed and for $\alpha = 60°$, only Category 1 was observed. It should be pointed out that the theory is only capable of predicting entrainment Categories 1, 3, and 5 only. In Fig. 11, the theory appears to predict the entrainment category extremely well. In Figs. 12 and 13, however, the simultaneous point (Category 3) appears to be overpredicted by the theory. Nonetheless, the theoretical predictions of h/d are in very good agreement with the data in Figs. 11–13.

The data for $L/d = 8$, shown in Figs. 14–16 demonstrate that when entrainment is occurring at branch 1, Fr_2 has no significant effect on h/d and when entrainment is occurring at branch 2, Fr_1 has no significant effect on h/d. This confirms the conclusion made earlier from the gas entrainment data that the branches behave independently for this configuration. Only three entrainment categories were observed (1, 3 and 5) for all values of α tested, and all categories shift to lower Fr_1 and α increases (similar to $L/d = 1.5$). The theory predicts the entrainment categories

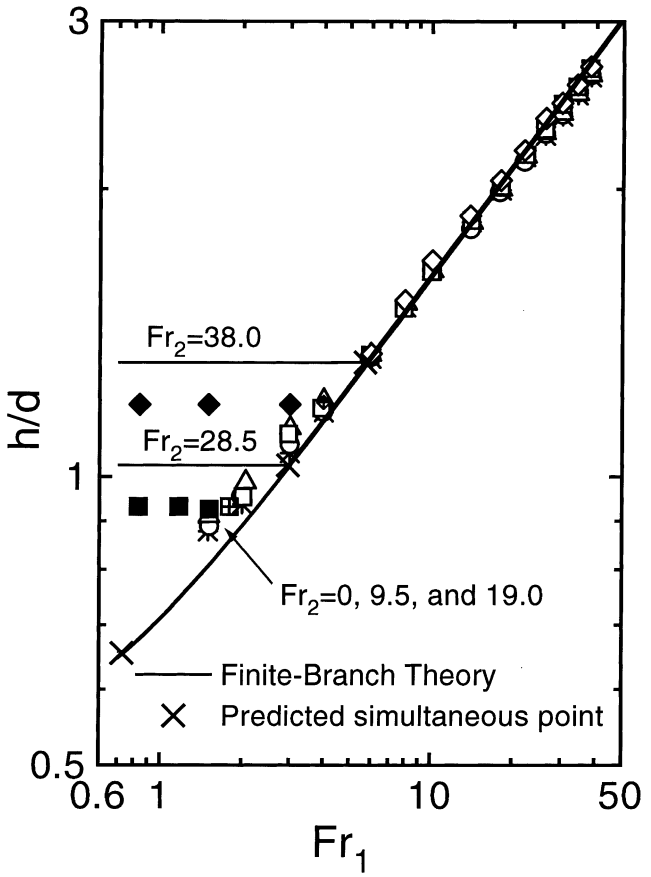

Fig. 15. Experimental data and theoretical predictions of liquid-entrainment for $L/d = 8.0$ and $\alpha = 10°$.

extremely well for $\alpha = 0°$ and reasonably well for $\alpha = 10°$. Both data and theory agree that only entrainment Category 1 is present for $\alpha = 30°$ under the test conditions used in Fig. 16. In general, the experimental values of h/d are predicted well by the theory.

3.5. Comparison with previous data

Several comparisons were made between the present data and previous data in order to ascertain the accuracy of the present data and the validity of the present experimental procedure. All comparisons resulted in good agreement (Maier, 1998) and a sample is shown in Figs. 17 and 18 for gas and liquid entrainment, respectively. These two comparisons are against the data of Hassan (1995) who considered only the condition $Fr_1 = Fr_2$ in his experiment with $\alpha = 0°$ and 90°. Figs. 17 and 18 correspond to $\alpha = 0°$ with various L/d, including the single-discharge case. Both figures show good agreement between the two sets of data for all values of L/d. For $L/d = 8$, both data sets converge to the single-branch condition.

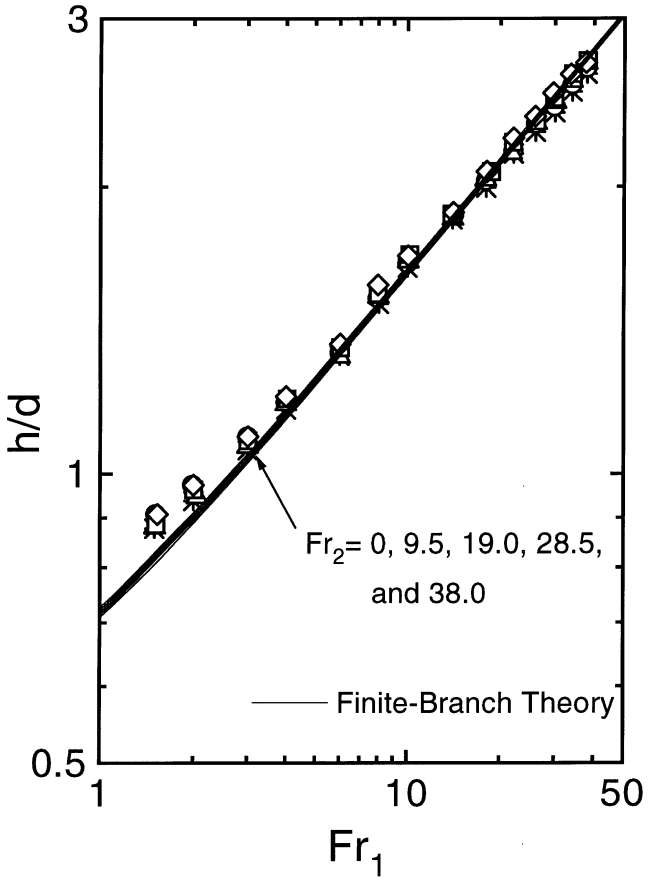

Fig. 16. Experimental data and theoretical predictions of liquid-entrainment for $L/d = 8.0$ and $\alpha = 30°$.

4. Concluding remarks

Experimental data were generated for the onset of gas and liquid entrainment for the case of two horizontal side circular branches of 6.35 mm diameter discharging from a large reservoir containing a stratified, two-phase mixture of air and water. The independent variables in the investigation included the separation distance L/d, the rate of discharge from each branch, Fr_1 and Fr_2, and the angular alignment of the branch centerlines, α. The dependent variables were the critical height at which the onset occurred, h/d, as measured from the flat, smooth air–water interface to the centreline of the branch closest to the interface, and the location of the onset of entrainment. The experimental data were collected at room temperature and a test section pressure of 510 kPa for gas entrainment and 310 kPa for liquid entrainment. For both the gas and liquid entrainment investigations, separation distance of $L/d = 1.5$, 2.0, and 8.0 were studied and angles of $\alpha = 0°, 10°, 30°$, and 60° were investigated. Measurements of the critical height were taken over a wide range of Froude numbers from the branches.

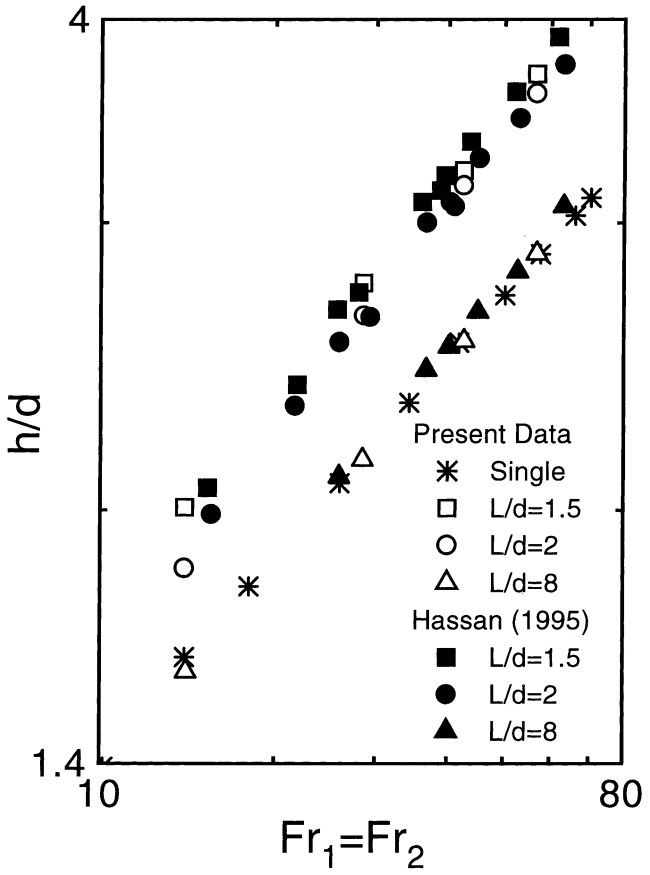

Fig. 17. Comparison of gas-entrainment data with Hassan (1995) for $\alpha = 0°$.

Based on visual observation, the experimental data for the onset of gas and liquid entrainment were classified into five distinct categories depending on the location at which the entrainment onset occurs. For low branch separation ($L/d = 1.5$ and 2.0), branch interaction was evident by the fact that the critical height was found to increase with an increase of either Fr_1 or Fr_2. While, for high branch separation ($L/d = 8.0$), the branches operated independently whereby Fr_1 had no significant effect on h/d if the entrainment was at branch 2 and Fr_2 had no significant effect on h/d if the entrainment was at branch 1. Generally, h/d increases as L/d decreases. Also, h/d was found to decrease as α increases, particularly if the onset of entrainment was occurring at branch 2. For the covered range of operating conditions, entrainment at branch 2 no longer occurred, or was limited to very low Fr_1, for: $\alpha = 60°$ with $L/d = 1.5$ and 2.0, and for $\alpha = 30°$ with $L/d = 8.0$ for both gas and liquid entrainment.

Comparisons were made between the present data on liquid entrainment and the finite-branch theoretical model developed in Part 1 of this paper. The model agreed very well with the experimental values of h/d. In terms of the onset location, the model performed generally well with a slight over-prediction of the simultaneous point under some operating conditions.

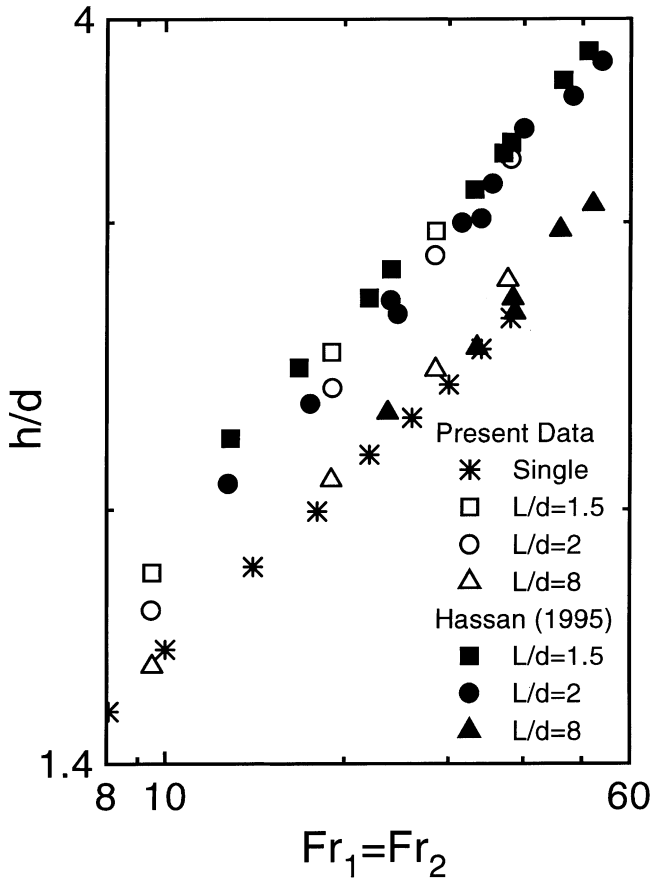

Fig. 18. Comparison of liquid-entrainment data with Hassan (1995) for $\alpha = 0°$.

Acknowledgements

The financial support provided by the Natural Sciences and Engineering Research Council of Canada is gratefully acknowledged.

References

Armstrong, K.F., Parrott, S.D., Sims, G.E., Soliman, H.M., Krishnan, V.S., 1992. Theoretical and experimental study of the onset of liquid entrainment during dual discharge from large reservoirs. Int. J. Multiphase Flow 18, 217–227.

Hassan, I.G., 1995. Single, dual and triple discharge from a large, stratified, two-phase region through small branches. Ph.D. thesis, University of Manitoba.

Hassan, I.G., Soliman, H.M., Sims, G.E., Kowalski, J.E., 1996a. Discharge from a smooth stratified two-phase region through two horizontal side branches located in the same vertical plane. Int. J. Multiphase Flow 22, 1123–1142.

Hassan, I.G., Soliman, H.M., Sims, G.E., Kowalski, J.E., 1996b. Experimental investigation of the two-phase discharge from a stratified region through two side branches oriented horizontally. Experimental Thermal Fluid Sci. 13, 117–128.

Hassan, I.G., Soliman, H.M., Sims, G.E., Kowalski, J.E., 1997. Single and multiple discharge from a stratified two-phase region through small branches. Nucl. Engrg. Des. 176, 233–245.

Hassan, I.G., Soliman, H.M., Sims, G.E., Kowalski, J.E., 1998. Two-phase flow from a stratified region through a small side branch. J. Fluids Engrg. 120, 605–612.

Kline, S.J., McClintock, F.A., 1953. Describing uncertainties in single-sample experiments. Mech. Engrg. 75, 3–8.

Maier, M.R., 1998. Onsets of liquid and gas entrainment during discharge from a stratified air–water region through two horizontal side branches with centrelines falling in an inclined plane. M.Sc. thesis, University of Manitoba.

Maier, M.R., Soliman, H.M., Sims, G.E., 2001. Onsets of entrainment during dual discharge from a stratified two-phase region through horizontal branches with centrelines falling in an inclined plane: Part 1 – Analysis of liquid entrainment. Int. J. Multiphase Flow 27, 1011–1028.

Micaelli, J.C., Memponteil, A., 1989. Two-phase flow behavior in a tee-junction: the CATHARE model. In: Proceedings of the Fourth International Topical Meeting on Nuclear Reactor Thermal-hydraulics, vol. 2. Karlsruhe, Germany, pp. 1024–1030.

Parrott, S.D., 1993. Experiments on the onsets of gas pull-through and liquid entrainment during dual discharge from a large reservoir. M.Sc. thesis, University of Manitoba.

Parrott, S.D., Soliman, H.M., Sims, G.E., Krishnan, V.S., 1991. Experiments on the onset of gas pull-through during dual discharge from a reservoir. Int. J. Multiphase Flow 17, 119–129.

Schrock, V.E., Revankar, S.T., Mannheimer, R., Wang, C.H., Jia, D., 1986. Steam-water critical flow through small pipes from stratified upstream regions. In: Proceedings of the Eighth International Heat Transfer Conference, vol. 5. San Francisco, CA, pp. 2307–2311.

Smoglie, C., Reimann, J., 1986. Two-phase flow through small branches in a horizontal pipe with stratified flow. Int. J. Multiphase Flow 12, 609–625.

Yonomoto, T., Tasaka, K., 1988. New theoretical model for two-phase flow discharged from stratified two-phase region through small break. J. Nucl. Sci. Technol. 25, 441–455.

Yonomoto, T., Tasaka, K., 1991. Liquid and gas entrainment to a small break hole from a stratified two-phase region. Int. J. Multiphase Flow 17, 745–765.